Journal of Luminescence 186 (2017) 170–174

Contents lists available at ScienceDirect

Journal of Luminescence

journal homepage: www.elsevier.com/locate/jlumin

Efficient energy back transfer from Ce^{3+} 5d state to Pr^{3+} $^1D_2$ level in $Lu_3Al_5O_{12}$ upon Pr^{3+} 4f5d excitation ☆

Dan Wu [a,b], Zhendong Hao [a], Xia Zhang [a], Guo-Hui Pan [a], Yongshi Luo [a], Ligong Zhang [a], Haifeng Zhao [a], Jiahua Zhang [a,*]

[a] State Key Laboratory of Luminescence and Applications, Changchun Institute of Optics, Fine Mechanics and Physics, Chinese Academy of Sciences, Changchun 130033, Jilin, China
[b] University of Chinese Academy of Sciences, Beijing 100049, China

ARTICLE INFO

Article history:
Received 5 July 2016
Received in revised form
29 December 2016
Accepted 2 February 2017
Available online 7 February 2017

ABSTRACT

The step energy transfers from Pr^{3+} 4f5*d* state to Ce^{3+} 5*d* state followed by energy back transfer from Ce^{3+} 5*d* state to Pr^{3+} $^1D_2$ level are studied. The $Ce^{3+}\rightarrow Pr^{3+}$ energy back transfer upon Pr^{3+} 4f5*d* excitation is found to be more efficient than the normal $Ce^{3+}\rightarrow Pr^{3+}$ energy transfer upon Ce^{3+} 5*d* excitation. The efficient energy back transfer is attributed to preferential excitation of the Ce^{3+} ion with an adjacent Pr^{3+} surrounding in $Pr^{3+}\rightarrow Ce^{3+}$ energy transfer of the first step, whereas Ce^{3+} is excited randomly in the normal energy transfer. The efficiencies of $Ce^{3+}\rightarrow Pr^{3+}$ energy back transfer as a function of Ce^{3+} and Pr^{3+} concentration are evaluated, respectively.

1. Introduction

Energy transfer followed by energy back transfer between luminescent centers considerably affects luminescent properties of luminescent materials and it has been observed in various rare earth ion pairs [1–3]. Ce^{3+} doped rare earth aluminium garnets e.g. Yttrium aluminium garnet (YAG) and Lutetium aluminium garnet (LuAG) exhibit highly efficient luminescence. These materials can serve as excellent phosphors for use in white light emitting diodes (*w*-LEDs) and high energy radiation detection [4–7]. Introducing Pr^{3+} into Ce^{3+} doped garnets can modify their luminescent properties through energy transfer between Ce^{3+} and Pr^{3+} [8,9]. In our previous work [10,11], we have studied $Ce^{3+}\rightarrow Pr^{3+}$ energy transfer upon Ce^{3+} 5*d* excitation at around 450 nm in YAG. The energy transfer results in the appearance of pronounced red emission line of Pr^{3+} $^1D_2\rightarrow{}^3H_4$ transition added into the yellow emission band of Ce^{3+} 5*d* → 4*f* transition, being helpful for the improvement of color rendering in YAG:Ce^{3+} converted *w*-LEDs. Yang and Kim have studied luminescent properties of YAG:Ce^{3+}, Pr^{3+} nanocrystalline phosphors [12]. They selected 287 nm wavelength to excite Pr^{3+} 4*f*5*d* state and observed both the red emission line of Pr^{3+} and the yellow emission band of Ce^{3+}. This result was attributed to two step energy transfers, i.e., from Pr^{3+} 4*f*5*d* to Ce^{3+} 5*d*, and from Ce^{3+} 5*d* back to Pr^{3+} $^1D_2$. The emission spectra also demonstrated that the intensity ratio of the red emission line to the yellow emission band upon Pr^{3+} excitation is larger than that upon Ce^{3+} 5*d* excitation. This phenomena is not yet explained.

LuAG is a good host for scintillation due to its higher density, effective atomic number (Z_{eff} = 62.9) and higher light yield compared with YAG [13–15]. Ogieglo et al. have codoped Pr^{3+} into LuAG:Ce^{3+} scintillator in attempt to increase the light yield as Pr^{3+} 4*f*5*d* state can efficiently capture the electron-hole pairs generated by radiation and subsequently transfer energy to Ce^{3+} 5*d* state. They also found that Ce^{3+} excited by energy transfer from Pr^{3+} can transfer energy back to Pr^{3+} to populate Pr^{3+} $^1D_2$ level [9]. However, the efficiency of the $Ce^{3+}\rightarrow Pr^{3+}$ energy back transfer has rarely been studied. In principle, the $Ce^{3+}\rightarrow Pr^{3+}$ energy back transfer upon Pr^{3+} 4*f*5*d* excitation should be more efficient than the $Ce^{3+}\rightarrow Pr^{3+}$ energy transfer upon Ce^{3+} 5*d* excitation. The reasons for that are as follows. Upon Pr^{3+} 4*f*5*d* excitation, Ce^{3+} is excited by energy transfer from Pr^{3+}, resulting in that the Ce^{3+} ion that has an adjacent Pr^{3+} surrounding is preferentially excited, i.e., preferential excitation of Ce^{3+} in the closely spaced Ce^{3+}-Pr^{3+} pairs, whereas direct photo-excitation of Ce^{3+} 5*d* undergoes random excitation of Ce^{3+}. As a result, the $Ce^{3+}\rightarrow Pr^{3+}$ energy back transfer should be more efficient than the $Ce^{3+}\rightarrow Pr^{3+}$ energy transfer.

In this paper, we study $Pr^{3+}\rightarrow Ce^{3+}\rightarrow Pr^{3+}$ step energy transfers in LuAG upon Pr^{3+} 4*f*5*d* excitation. The efficient $Ce^{3+}\rightarrow Pr^{3+}$ energy

☆This work highlights that the energy back transfer from Ce^{3+} 5d state to Pr^{3+} $^1D_2$ level after the Ce^{3+} 5d state is populated by energy transfer from Pr^{3+}.

* Corresponding author.
E-mail address: zhangjh@ciomp.ac.cn (J. Zhang).

http://dx.doi.org/10.1016/j.jlumin.2017.02.002
0022-2313/

back transfer with respect to the $Ce^{3+} \rightarrow Pr^{3+}$ energy transfer is observed. The efficiencies of these energy transfers as a function of Ce^{3+} and Pr^{3+} concentration are evaluated, respectively.

2. Experimental

The powder phosphor samples were synthesized by the high temperature solid-state reaction with mixtures of high-purity Lu_2O_3, CeO_2, Al_2O_3, and Pr_6O_{11} in molar of $(Lu_{1-x-y}Ce_xPr_y)_3Al_5O_{12}$ (x, y represent the concentration of Ce^{3+}, Pr^{3+}, respectively), 3 wt% AlF_3 was appended as the flux. After a good mixing in an agate mortar, the mixtures were sintered under CO reducing condition at 1550 °C for 5 h. The structure of the final products was characterized by powder X-ray diffraction (XRD). Room temperature photoluminescence (PL) and photoluminescence excitation (PLE) spectra were measured with a Hitachi Spectrometer (F-7000). The fluorescence decays of Ce^{3+} were measured by an FL920 fluorimeter (Edinburgh Instruments, Livingston, UK) with a hydrogen flash lamp (nF900; Edinburgh Instruments). All the measurements were conducted at room temperature.

3. Results and discussion

Fig. 1 shows the XRD patterns of $(Lu_{(1-x-y)}Ce_xPr_y)_3Al_5O_{12}$ samples. It is obvious that all the diffraction peaks of the samples can be well indexed to the cubic phase (JCPDS no. 73–1368) and no detectable impurities are present, indicating that doping Ce^{3+} and Pr^{3+} does not generate any impurities or induce significant changes in the host structure.

The PLE and PL spectra for $(Lu_{0.99}Ce_{0.01})_3Al_5O_{12}$ (a), $(Lu_{0.995}Pr_{0.005})_3Al_5O_{12}$ (b), $(Lu_{0.985}Ce_{0.01}Pr_{0.005})_3Al_5O_{12}$ (c) are shown in Fig. 2. The Ce^{3+} singly doped sample exhibits a broad green emission band around 545 nm, which originates from the transition of the lowest-lying 5*d* state to the 4*f* ground state of Ce^{3+}. Meanwhile, the PLE spectrum of the green emission consists of two strong bands located around 445 nm and 350 nm, which originates from the transitions of the 4*f* ground state to the lowest and upper 5*d* states of Ce^{3+}, respectively [16]. The PL spectrum of Pr^{3+} singly doped sample upon 285 nm excitation exhibits several emission bands (see Fig. 2(b)). In the UV region, the two strong emission bands peaked at 310 nm and 372 nm are assigned to the transitions from the lowest-lying 4*f*5*d* state to ^3H_J (J=4, 5, 6) and ^3F_J (J=2, 3, 4) levels, respectively. There are also two weak emission lines at 488 nm and 610 nm, which are assigned to $^3P_0 \rightarrow {}^3H_4$ and $^1D_2 \rightarrow {}^3H_4$ transitions, respectively. The PLE spectrum of the red emission line contains three groups of excitations in Pr^{3+} singly doped sample. In the UV spectral region the bands located at 285 nm and 242 nm are due to the $4f \rightarrow 5d$ transitions of Pr^{3+}. The lines in the range of 430 nm-500 nm are attributed to $^3H_4 \rightarrow {}^3P_J$ (J = 0, 1, 2), $^1I_6$ transitions. The excitation lines around 600 nm originates from $^3H_4 \rightarrow {}^1D_2$ transition. In Ce^{3+} and Pr^{3+} codoped sample, as shown in Fig. 2(c), the PLE spectrum for monitoring the Ce^{3+} emission at 545 nm appears remarkable 4*f*5*d* bands of Pr^{3+} peaking at 242 and 285 nm. This indicates the existence of energy transfer from Pr^{3+} 4*f*5*d* state to Ce^{3+} 5*d* state. When only Ce^{3+} is excited at 430 nm, the PL spectrum contains not only the green band of Ce^{3+} but also an intense red emission line of Pr^{3+} at 610 nm, indicating the occurrence of energy transfer from Ce^{3+} 5*d* state to Pr^{3+} $^1D_2$ level.

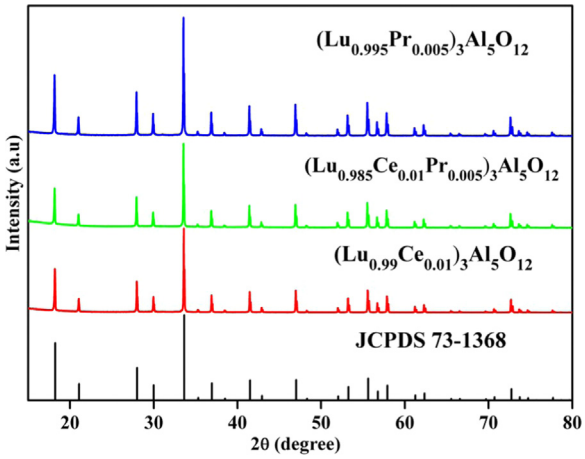

Fig. 1. The XRD patterns of $(Lu_{0.99}Ce_{0.01})_3Al_5O_{12}$, $(Lu_{0.985}Ce_{0.01}\ Pr_{0.005})_3Al_5O_{12}$ and $(Lu_{0.995}Pr_{0.005})_3Al_5O_{12}$.

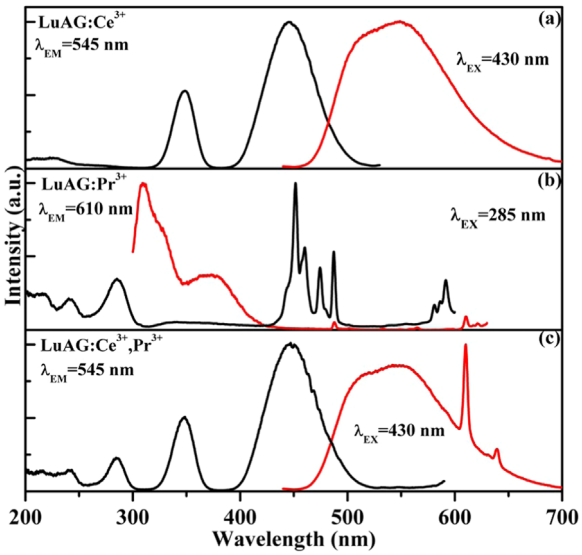

Fig. 2. PL and PLE spectra of $(Lu_{0.99}Ce_{0.01})_3Al_5O_{12}$, $(Lu_{0.995}Pr_{0.005})_3Al_5O_{12}$ and $(Lu_{0.985}Ce_{0.01}\ Pr_{0.005})_3Al_5O_{12}$.

Fig. 3 shows the PL spectra of sample series A: $(Lu_{0.995-x}Ce_xPr_{0.005})_3Al_5O_{12}$, with a fixed Pr^{3+} concentration at 0.005 and various Ce^{3+} concentrations ranging from 0 to 0.02 upon Pr^{3+} 4*f*5*d* excitation at 285 nm (solid) and/or upon Ce^{3+} 5*d* excitation at 430 nm (dotted). Upon Pr^{3+} 4*f*5*d* excitation in Pr^{3+} singly doped sample, the 4*f*5*d* emission bands in the UV spectral region dominate the PL spectrum with a weak $^3P_0 \rightarrow {}^3H_4$ blue emission line at 488 nm and a $^1D_2 \rightarrow {}^3H_4$ red emission line at 610 nm. With addition of Ce^{3+}, the UV emission bands and the blue emission line of Pr^{3+} are weakened with the appearance of the strong green emission band of Ce^{3+} and the strongly enhanced red emission line of Pr^{3+}. In Pr^{3+} singly doped sample, the blue emission line and the red emission line are very weak with respect to the UV emission bands, indicating that the rate of nonradiative relaxation from the 4*f*5*d* state down to the $^3P_0$ and $^1D_2$ levels is much smaller than the radiative rate of the 4*f*5*d* emission [17]. If the nonradiative relaxation rate is independent of Ce^{3+} addition, the intensity ratio of the blue and/or the red emission line to the UV emission should keep unchanged in the presence of Ce^{3+}. This is evidenced by the intensity reduction of both the UV and the blue emission in the presence of Ce^{3+}. The strong enhancement of the red emission line with respect to both the UV and the blue emission in the presence of Ce^{3+} is attributed to the step energy transfers, that is, energy transfer from Pr^{3+} 4*f*5*d* state to Ce^{3+} 5*d* state and energy back transfer from Ce^{3+} 5*d* state to Pr^{3+} $^1D_2$ level. The two step energy transfers open an additional route for populating the Pr^{3+} $^1D_2$ level from Pr^{3+} 4*f*5*d* state with the use of Ce^{3+} 5*d* as an intermediate state, as sketched in Fig. 4.

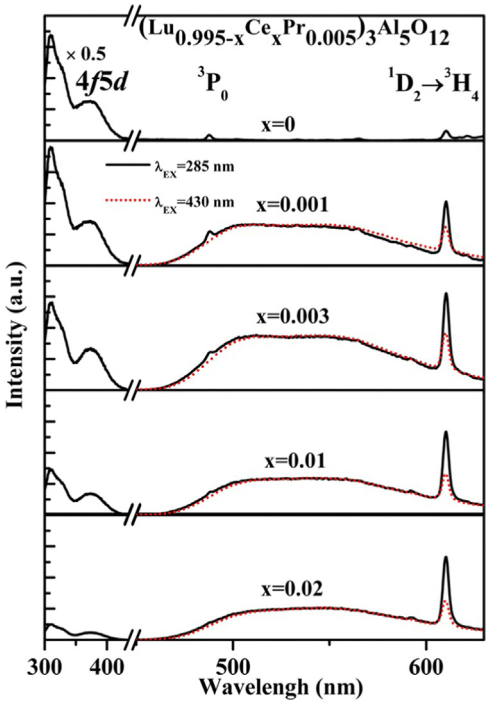

Fig. 3. PL spectra of sample series A: $(Lu_{0.995-x}Ce_xPr_{0.005})_3Al_5O_{12}$, ($x$=0–0.02) upon Pr^{3+} 4*f*5*d* excitation at 285 nm (solid), and/or upon Ce^{3+} 5*d* excitation at 430 nm (dotted).The intensity of the Ce^{3+} emission band for 430 nm excitation is scaled to that for 285 nm excitation.

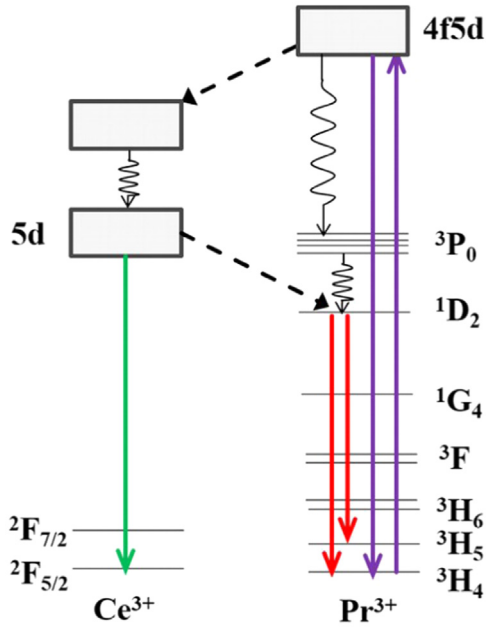

Fig. 4. Energy level diagrams of Ce^{3+} and Pr^{3+} with the possible pathways of $Pr^{3+}\rightarrow Ce^{3+}\rightarrow Pr^{3+}$ step energy transfers.

A notable result in Fig. 3 is that the intensity ratio of the red emission line of Pr^{3+} to the green emission band of Ce^{3+}, R/G ratio, for Pr^{3+} 4*f*5*d* excitation at 285 nm is always larger than that for Ce^{3+} 5*d* excitation at 430 nm. In view of negligible contribution of the nonradiative relaxation from Pr^{3+} 4*f*5*d* to the red emission line, the enhancement of the red emission indicates that the $Ce^{3+}\rightarrow Pr^{3+}$ energy back transfer is more efficient than the $Ce^{3+}\rightarrow Pr^{3+}$ energy transfer. This feature can be well explained as preferential excitation of Ce^{3+} in the closely spaced Ce^{3+}-Pr^{3+} pairs due to the first step $Pr^{3+}\rightarrow Ce^{3+}$ energy transfer upon Pr^{3+}

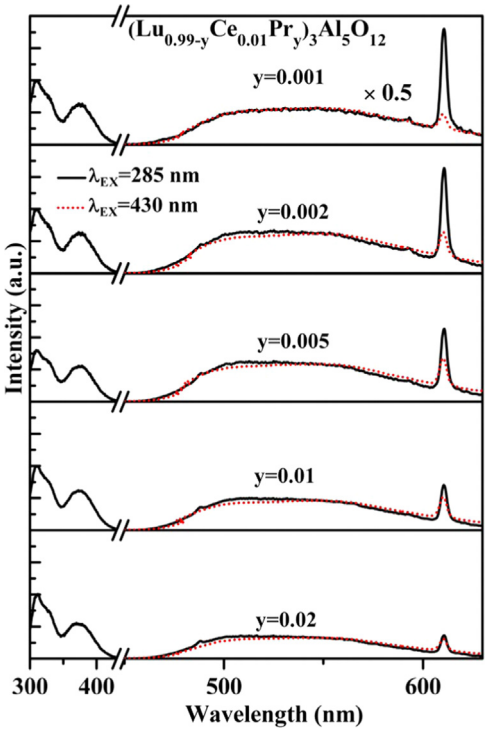

Fig. 5. PL spectra of $(Lu_{0.99-y}Ce_{0.01}Pr_y)_3Al_5O_{12}$, ($y$=0.001–0.02) upon Pr^{3+} 4*f*5*d* excitation at 285 nm (solid), and/or upon Ce^{3+} 5*d* excitation at 430 nm (dotted). The intensity of the Ce3+ emission band for 430 nm excitation is scaled to that for 285 nm excitation.

4*f*5*d* excitation. Here, we define n by

$$n=\frac{(R/G)_{Pr^{3+}4f5d}}{(R/G)_{Ce^{3+}5d}} \quad (1)$$

The subscript (Pr^{3+} 4*f*5*d* or Ce^{3+} 5*d*) indicates the excitation level for which the R/G ratio is obtained. One can find from Fig. 3 that the n values increase with increasing Ce^{3+} concentration up to 0.02.

For comparison the emission spectra of sample series B: $(Lu_{0.99-y}Ce_{0.01}Pr_y)_3Al_5O_{12}$, ($y$=0.001–0.02) with a fixed Ce^{3+} concentration at 0.01 and various Pr^{3+} concentrations are also measured, as shown in Fig. 5. Obviously, there is a high n value for low Pr^{3+} concentration and it reduces with increasing Pr^{3+} concentration.

From the definition of n, its value is determined by η_{ET}, the efficiency of $Ce^{3+}\rightarrow Pr^{3+}$ energy back transfer upon Pr^{3+} 4*f*5*d* excitation, and η'_{ET}, the efficiency of $Ce^{3+}\rightarrow Pr^{3+}$ energy transfer upon Ce^{3+} 5*d* excitation, written as

$$n=\frac{(R/G)_{Pr^{3+}4f5d}}{(R/G)_{Ce^{3+}5d}}=\frac{\left(\frac{\eta_{ET}\eta_A}{1-\eta_{ET}}\right)_{Pr^{3+}4f5d}}{\left(\frac{\eta'_{ET}}{1-\eta'_{ET}}\right)_{Ce^{3+}5d}} \quad (2)$$

where η_A is the radiative efficiency of Pr^{3+}:$^1D_2$ level, which is a conctant and does not change with the excitation wavelength. To calculate η_{ET}, η'_{ET} must be obtained first. As shown in Fig. 6(a) and (b), the decay curves of Ce^{3+} emission upon Ce^{3+} 5*d* excitation are measured for both the sample series A: $(Lu_{0.995-x}Ce_xPr_{0.005})_3Al_5O_{12}$, ($x$=0.001–0.02) and the sample series B: $(Lu_{0.99-y}Ce_{0.01}Pr_y)_3Al_5O_{12}$, ($y$=0.001–0.02). For comparison, the decay curves of Ce^{3+} emission upon Pr^{3+} 4*f*5*d* excitation are also shown in Fig. 7(a) and (b). Upon Ce^{3+} 5*d* excitation, the decay becomes faster with increasing the dopant concentrations due to energy transfer from Ce^{3+} to Pr^{3+}. However, one can find from Fig. 7 that the decay curves of Ce^{3+}

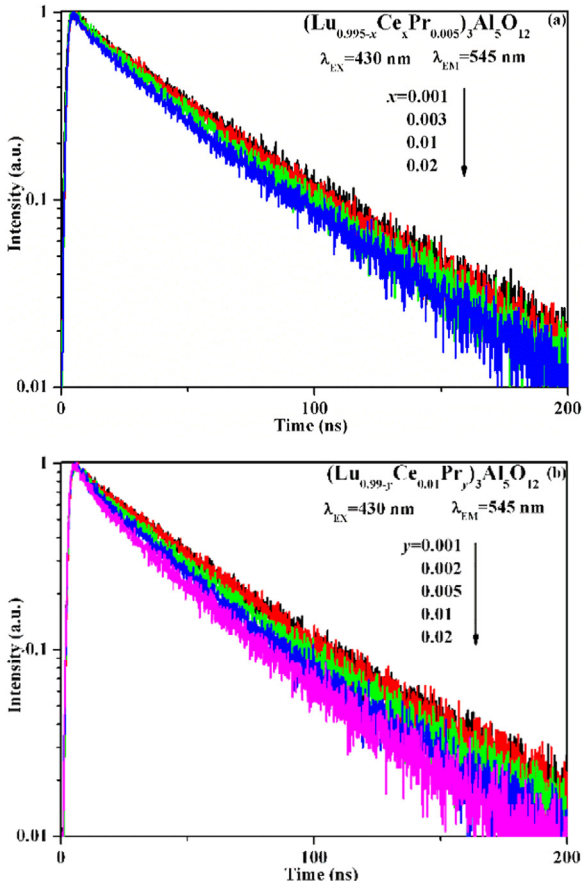

Fig. 6. Decay curves of Ce^{3+} emission in $(Lu_{0.995-x}Ce_xPr_{0.005})_3Al_5O_{12}$, ($x$=0.001–0.02) (a) and $(Lu_{0.99-y}Ce_{0.01}Pr_y)_3Al_5O_{12}$, ($y$=0.001–0.02) (b) upon Ce^{3+} 5*d* excitation at 430 nm.

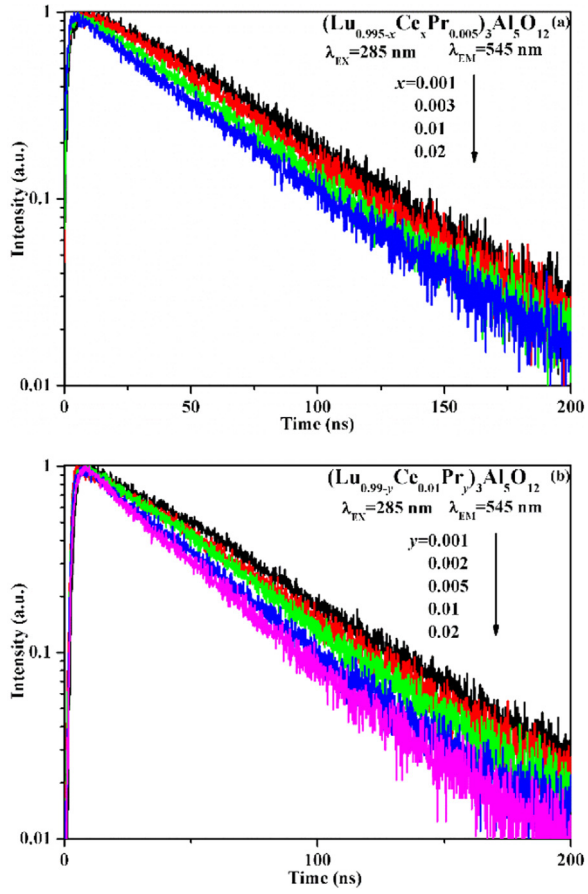

Fig. 7. Decay curves of Ce^{3+} emission in $(Lu_{0.995-x}Ce_xPr_{0.005})_3Al_5O_{12}$, ($x$=0.001–0.02) (a) and $(Lu_{0.99-y}Ce_{0.01}Pr_y)_3Al_5O_{12}$, ($y$=0.001–0.02) (b) upon Pr^{3+} 4*f*5*d* excitation at 285 nm.

upon Pr^{3+} 4*f*5*d* excitation do not appear a fast decay compared with that upon Ce^{3+} direct excitation. It seems inconsistent with the efficient energy back transfer from Ce^{3+} to Pr^{3+}. This behaviour can be understood considering the existence of population build up process of Ce^{3+} emission due to energy transfer from Pr^{3+} to Ce^{3+}. We can see the rising time when Ce^{3+} emission reaches the maximum upon Pr^{3+} 4*f*5*d* excitation is continuously reduced with the increase of dopant concentrations, reflecting that the energy transfer from Pr^{3+} to Ce^{3+} continuously shortens the lifetime of Pr^{3+} 4*f*5*d* level. Although the rising time is shown to be shorter than 10 ns, the slow rising edge followed with slow decay contributed by distant Pr^{3+}-Ce^{3+} are still hidden in the temporal behaviour. As a result, the expected fast decay of Ce^{3+} upon Pr^{3+} 4*f*5*d* excitation may be covered by the slow build up and decay processes, leading to a slow decay pattern.

The transfer efficiency upon Ce^{3+} 5*d* excitation can be given by [18]

$$\eta'_{ET} = 1 - \int_0^\infty I(t)dt/\tau_0 \quad (3)$$

where $I(t)$ is the Ce^{3+} fluorescence decay function with a unit initial intensity; τ_0 is the fluorescence lifetime of Ce^{3+} in the absence of Pr^{3+}. The calculated energy back transfer efficiencies using Eq. (2) are listed in Table 1 and Table 2.

From Tables 1 and 2, one can find that the n values increase with increasing Ce^{3+} concentration for sample series A and decrease with increasing Pr^{3+} concentration for sample series B. As mentioned above, the photon-excitation of Pr^{3+} 4*f*5*d* state can lead to preferential excitation of Ce^{3+} in the closely spaced Ce^{3+}-Pr^{3+} pairs by $Pr^{3+} \rightarrow Ce^{3+}$ energy transfer. For the sample series A, the average distance between the excited Ce^{3+} and it's adjacent Pr^{3+} upon Pr^{3+} 4*f*5*d* excitation becomes shorter with the increase of Ce^{3+} concentration, thus enhancing the $Ce^{3+} \rightarrow Pr^{3+}$ energy back transfer rate. Whereas, the photon-excitation of Ce^{3+} 5*d* has no selectivity for the Ce^{3+}-Pr^{3+} distance and the average distance for $Ce^{3+} \rightarrow Pr^{3+}$ energy transfer is unchanged with

Table 1
Fluorescent lifetimes and transfer efficiencies in Samples A: $(Lu_{0.995-x}Ce_xPr_{0.005})_3Al_5O_{12}$.

x	$\int_0^\infty I(t)dt$ (ns)	τ_0 (ns)	η'_{ET}	*n*	η_{ET}
0.001	46.8	56.5	0.17	1.9	0.28
0.003	43.4	54.1	0.2	2.0	0.33
0.01	36.8	45.4	0.19	2.2	0.34
0.02	35.0	41.6	0.16	2.8	0.35

Table 2
Fluorescent lifetimes and transfer efficiencies in Samples B: $(Lu_{0.99-y}Ce_{0.01}Pr_y)_3Al_5O_{12}$.

y	$\int_0^\infty I(t)dt$ (ns)	η'_{ET}	*n*	η_{ET}
0	45.4			
0.001	42.8	0.06	6.5	0.29
0.002	40.8	0.1	3.8	0.30
0.005	36.8	0.19	2.2	0.34
0.01	33.4	0.26	1.5	0.35
0.02	27.8	0.39	1.2	0.43

changing Ce^{3+} concentration. For the sample series B, the average rate for the $Ce^{3+} \rightarrow Pr^{3+}$ energy transfer upon Ce^{3+} 5*d* excitation is proportional to Pr^{3+} concentration. While the $Ce^{3+} \rightarrow Pr^{3+}$ energy back transfer upon Pr^{3+} 4*f*5*d* excitation includes transfer from Ce^{3+} to the close Pr^{3+} and the distant Pr^{3+}. At low concentration of Pr^{3+}, the $Ce^{3+} \rightarrow Pr^{3+}$ energy transfer rate upon Ce^{3+} 5*d* excitation is low simultaneously, however, the $Ce^{3+} \rightarrow Pr^{3+}$ energy back transfer is still effective due to the back transfer to the close Pr^{3+}, the rate of which is independent of Pr^{3+} concentration. As a result, there is a big *n* value for low concentration of Pr^{3+}. With increasing Pr^{3+} concentration, the average rate for the $Ce^{3+} \rightarrow Pr^{3+}$ normal energy transfer is increased, while the average rate for the $Ce^{3+} \rightarrow Pr^{3+}$ back transfer is also increased because the back transfer from Ce^{3+} to distant Pr^{3+} ions becomes more and more important and even dominates the overall transfer for a sufficient high concentration of Pr^{3+}. Hence, the *n* values reduce with the increase of Pr^{3+} concentration and it is expected to be 1 at high Pr^{3+} concentration similar to the case for Pr^{3+} concentration of 0.02 with $n = 1.2$ in this work.

4. Conclusions

In summary, Upon Pr^{3+} 4*f*5*d* state excitation, the step energy transfers from Pr^{3+} 4*f*5*d* state to Ce^{3+} 5*d* state followed by energy back transfer from Ce^{3+} 5*d* state to Pr^{3+} $^1D_2$ level are studied in $Lu_3Al_5O_{12}$ (LuAG). The back transfer results in strongly enhanced red emission line of Pr^{3+} in the codoped sample compared with Pr^{3+} singly doped sample. The efficiencies of $Ce^{3+} \rightarrow Pr^{3+}$ energy back transfer are evaluated. It is evidently found that the $Ce^{3+} \rightarrow Pr^{3+}$ energy back transfer upon Pr^{3+} 4*f*5*d* state excitation is more efficient than the normal $Ce^{3+} \rightarrow Pr^{3+}$ energy transfer upon Ce^{3+} 5*d* state excitation. The *n* values increase with increasing Ce^{3+} concentration and decrease with increasing Pr^{3+} concentration. As discussed, the LuAG:Ce^{3+},Pr^{3+} phosphors can serve as a model system for providing theoretical understanding of the step energy transfers, and the identification of the importance of this mechanism in other material hosts is expected.

Acknowledgements

This work is financially supported by the National Natural Science Foundation of China (61275055, 11274007, 51402284), the Natural Science Foundation of Jilin Province (20140101169JC, 20150520022JH, 20160520171JH) and the Prior Sci-tech Program of Innovation and Entrepreneurship of Oversea Chinese Talent of Jilin province.

References

[1] J. Zhang, Z. Hao, J. Li, X. Zhang, Y. Luo, G. Pan, Light: Sci. Appl. 4 (2015) e239.
[2] G. Özen, J.P. Denis, P. Goldner, X. Wu, M. Genotelle, F. Pellé, Appl. Phys. Lett. 62 (1993) 928.
[3] W. Zheng, H. Zhu, R. Li, D. Tu, Y. Liu, W. Luo, X. Chen, Phys. Chem. Chem. Phys. 14 (2012) 6974.
[4] M. Shang, C. Li, J. Lin, Chem. Soc. Rev. 43 (2014) 1372.
[5] J.H. Oh, S.J. Yang, Y.R. Do, Light: Sci. Appl. 3 (2014) e141.
[6] A.A. Setlur, W.J. Heward, M.E. Hannah, U. Happek, Chem. Mater. 20 (2008) 6277.
[7] C. Greskovich, S. Duclos, Annu. Rev. Mater. Sci. 27 (1997) 69.
[8] R. Mueller-Mach, G.O. Mueller, M.R. Krames, T. Trottier, Sel. Top. Quantum Electron. IEEE J. 8 (2002) 339.
[9] J.M. Ogiegło, A. Zych, T. Jüstel, A. Meijerink, C.R. Ronda, Opt. Mater. 5 (2013) 322.
[10] L. Wang, X. Zhang, Z. Hao, Y. Luo, J. Zhang, X.J. Wang, J. Appl. Phys. 108 (2010) 093515.
[11] L. Wang, X. Zhang, Z. Hao, Y. Luo, X.J. Wang, J. Zhang, Opt. Express 18 (2010) 25177.
[12] H. Yang, S.Y. Kim, J. Lumin. 128 (2008) 1570.
[13] M. Nikl, E. Mihokova, J.A. Mareš, A. Vedda, M. Martini, K. Nejezchleb, K. Blažek, Physica Status Solidi (a) 181 (2000) R10.
[14] M. Nikl, H. Ogino, A. Krasnikov, A. Beitlerova, A. Yoshikawa, T. Fukuda, Physica Status Solidi (a) 202 (2005) R4.
[15] J.M. Ogiegło, A. Zych, K.V. Ivanovskikh, T. Jüstel, C.R. Ronda, A. Meijerink, J. Phys. Chem. A 116 (2012) 8464.
[16] M. Malinowski, P. Szczepanski, W. Wolinski, R. Wolski, Z. Frukacz, J. Phys.: Condens. Matter 5 (1993) 6469.
[17] J.M. Weber, Solid State Commun. 12 (1973) 741.
[18] M. Inokuti, F. Hirayama, J. Chem. Phys. 43 (1965) 1978.